

RESEARCH ARTICLE

10.1002/2015JD024568

Key Points:

- Real-time measurements of aerosol species were conducted at a rural site on Long Island, NY
- Urban emissions strongly influenced aerosol concentration and composition at this rural site
- Enhanced SOA formation was observed in mixed anthropogenic and biogenic emissions

Supporting Information:

- Supporting Information S1

Correspondence to:

Q. Zhang,
dkwzhang@ucdavis.edu

Citation:

Zhou, S., S. Collier, J. Xu, F. Mei, J. Wang, Y.-N. Lee, A. J. Sedlacek III, S. R. Springston, Y. Sun, and Q. Zhang (2016), Influences of upwind emission sources and atmospheric processing on aerosol chemistry and properties at a rural location in the Northeastern U.S., *J. Geophys. Res. Atmos.*, *121*, 6049–6065, doi:10.1002/2015JD024568.

Received 25 NOV 2015

Accepted 26 APR 2016

Accepted article online 29 APR 2016

Published online 19 MAY 2016

Influences of upwind emission sources and atmospheric processing on aerosol chemistry and properties at a rural location in the Northeastern U.S.

Shan Zhou¹, Sonya Collier¹, Jianzhong Xu^{1,2}, Fan Mei^{3,4}, Jian Wang³, Yin-Nan Lee³, Arthur J. Sedlacek III³, Stephen R. Springston³, Yele Sun^{1,5}, and Qi Zhang¹

¹Department of Environmental Toxicology, University of California, Davis, California, USA, ²Now at Cold and Arid Regions Environmental and Engineering Research Institute, Chinese Academy of Sciences, Lanzhou, China, ³Brookhaven National Laboratory, Upton, New York, USA, ⁴Now at Pacific Northwest National Laboratory, Richland, Washington, USA, ⁵Now at Institute of Atmospheric Physics, Chinese Academy of Sciences, Beijing, China

Abstract Continuous real-time measurements of atmospheric aerosol with an Aerodyne high-resolution time-of-flight aerosol mass spectrometer coupled with a fast temperature-stepping thermodenuder were carried out in summer 2011 at Brookhaven National Laboratory (BNL, 40.871°N, 72.89°W) during the Department of Energy Aerosol Life Cycle Intensive Operational Period campaign. BNL was frequently downwind of emissions from the New York metropolitan area and was exposed to various combinations of anthropogenic, biogenic, and marine emissions based on air mass history. The average concentration of submicrometer aerosol (PM₁) during this study was 12.6 μg m⁻³ with 64% of the mass being organic. Organic aerosol (OA) at BNL was found to be overwhelmingly secondary, consisting of (1) a fresher, semivolatile oxygenated organic aerosol (SV-OOA; oxygen-to-carbon ratio (O/C) = 0.54; 63% of OA mass) that was strongly influenced by transported urban plumes; (2) a regional, more aged, low-volatility OOA (LV-OOA; O/C = 0.97; 29% of OA mass) influenced by aqueous-phase processing; and (3) a nitrogen-enriched OA (NOA; nitrogen-to-carbon ratio (N/C) = 0.185; 8% of OA mass) likely composed of amine salts formed from acid-base reactions in industrial emissions. Urban emissions from the New York metropolitan areas to the W and SW in particular led to elevated PM₁ mass concentration and altered aerosol composition at BNL. Transported urban plumes and local biogenic emissions likely interacted to enhance secondary organic aerosol production, primarily represented by SV-OOA. These results suggest an important role that urban anthropogenic emissions play in affecting ambient PM concentration, composition, and physical-chemical properties at rural areas in the Northeast U.S.

1. Introduction

Aerosols significantly influence the radiative budget of the Earth's atmosphere [Ghan and Schwartz, 2007; Intergovernmental Panel on Climate Change (IPCC), 2013] and adversely affect human health [Pope and Dockery, 2006]. The properties and impacts of aerosols are intrinsically linked to the chemical composition of the particles, which is controlled by processes such as emissions of primary aerosols, formation of secondary species, and atmospheric aging. A thorough understanding of aerosol composition and lifecycle processes is crucial for improving the ability of models to accurately project future climate for different emission scenarios [IPCC, 2013].

Aerosols in densely populated urban environments are particularly concerning for their adverse effects on human health and air quality. The influences of urban pollution can also be expected at surrounding areas, especially downwind of the urban centers. Furthermore, urban pollutants tend to evolve and potentially form secondary species during transport, resulting in increased concentration of background pollutants on a regional scale. A number of studies have examined the influence of urban emissions on aerosol concentration and composition as they are diluted into the regional atmosphere. For example, Crippa *et al.* [2013] and Freutel *et al.* [2013] found that plumes from Paris exerted a significant influence onto its surroundings and that transported primary emissions could be observed while secondary organic aerosol (SOA) was not significantly influenced. Other studies, however, have shown substantial increases of SOA in urban plumes as they are processed, likely due to the interaction between urban plumes and biogenic VOC emissions [e.g., de Gouw *et al.*, 2005; DeCarlo *et al.*, 2010; Freney *et al.*, 2014; Kleinman *et al.*, 2008; Liggio *et al.*, 2010; Setyan *et al.*, 2012; Shilling *et al.*, 2013].

The Northeast megalopolis, which runs primarily northeast to southwest from Boston, Massachusetts, to Washington, DC, is the most highly urbanized region of the United States with intense urban and industrial emissions. This area is of particular importance to understanding aerosol lifecycle processes in the eastern U.S., where high concentrations of aerosols occur on a regional scale and are impacted by high anthropogenic and biogenic sources as well as long-range transported biomass burning plumes and marine aerosols. A number of previous studies have investigated aerosol composition and characteristics in the New York metropolitan area (NYMA) and found that primary organic aerosol (POA) contributes a large fraction, particularly near sources such as busy freeways; however, secondary sources can still form a dominant fraction of aerosol within NYMA, with sulfate and oxygenated organic aerosol (OOA) being dominant submicron aerosol (PM_{10}) components [e.g., *Drewnick et al.*, 2004a; *Massoli et al.*, 2012; *Sun et al.*, 2011, 2012b; *Weimer et al.*, 2006]. Airborne measurements in the eastern U.S. have also found that urban outflow resulted in aerosol dominated by sulfate and organic matter and that the latter was likely the major cause of regional haze [Bates et al., 2005; Peltier et al., 2007]. In addition, at a rural site in New Hampshire, the impact of urban outflow was observed and a combination of biogenic and anthropogenic emissions was found to have enhanced overall SOA formation [Cottrell et al., 2008].

During the summer of 2011, a Department of Energy (DOE) sponsored field campaign commonly referred to as Aerosol Lifecycle Intensive Observational Period (ALC-IOP) was conducted at the Brookhaven National Laboratory (BNL) in east-central Long Island, NY. A main goal of this campaign was to examine the evolution of aerosol properties and its dependence on atmospheric processing, meteorological conditions, and emission sources. Long Island is an excellent location to study the confluence of anthropogenic, biogenic, and marine emissions. It frequently receives urban emission-dominated air from the west and southwest (e.g., New York City ~80 km away and Washington D.C. ~ 430 km away) and biogenic emission-dominated air from the north and northeast with a distance from the source regions corresponding to atmospheric transport time of hours to days. Absent strong synoptic forcing, a sea breeze develops in the afternoon, introducing emissions from marine sources. In addition, long-range transport of intense but distant biomass burning events from North-central U.S./South-central Canada can occur in association with winds from the Northwest air masses [Sedlacek et al., 2012; Vladutescu et al., 2013]. Hence, this location and its specific conditions allow for the detailed investigation of aerosol chemistry and processing from various types of emission sources in the eastern U.S.

Here we provide an overview of PM_{10} characteristics at BNL based on the observations made by a high-resolution time-of-flight aerosol mass spectrometer (HR-AMS) coupled with a suite of collocated real-time measurements of aerosol properties, gas phase species, and meteorological conditions. The sources of OA are investigated via factor analysis of the HR-AMS data, and the influences of different emissions and atmospheric processing on aerosol characteristics are discussed together with back trajectory air mass analysis. We also examine the enhancement of SOA formation in the urban outflow upon mixing with intense biogenic emissions by comparing our results with previous observations made in NYC.

2. Methods

2.1. Campaign Site and Instrumentation

Measurements were made from 15 July to 15 August 2011 at the BNL "MetField"—a large open area that has been used over many decades for meteorological monitoring and occasionally for chemical measurements. The site (40.871°N, 72.89°W) is located ~80 km east of New York City and situated in an area characterized by pine-oak forests and small urban townships, with the Atlantic Ocean 25 km to the south and Long Island Sound (an estuary of the Atlantic Ocean) 16 km to the north (Figure 1a). The Long Island Expressway (I-495) is located approximately 3 km to the south of the sampling site.

During ALC-IOP a mobile laboratory was deployed containing an HR-AMS, for the size-resolved chemical characterization of nonrefractory (NR) PM_{10} ; a thermodenuder (TD), for aerosol volatility; a scanning mobility particle sizer (SMPS), for the size distribution of particles in the size range of 10–610 nm (in mobility diameter, D_m) divided into 60 size bins; and a size-resolved cloud condensation nuclei counter (Mei et al., in preparation). Prior to instrument sampling, ambient air was first directed through a 4 m long ½ inch copper tube at a flow rate of 12 lpm (liters-per-minute) with a $PM_{2.5}$ cyclone (URG Corporation), followed by a ¼ inch Nafion dryer and a 2 m long ¼ inch copper tube at 2 lpm. Particles have a residence time of 17 s in this inlet. Based on the

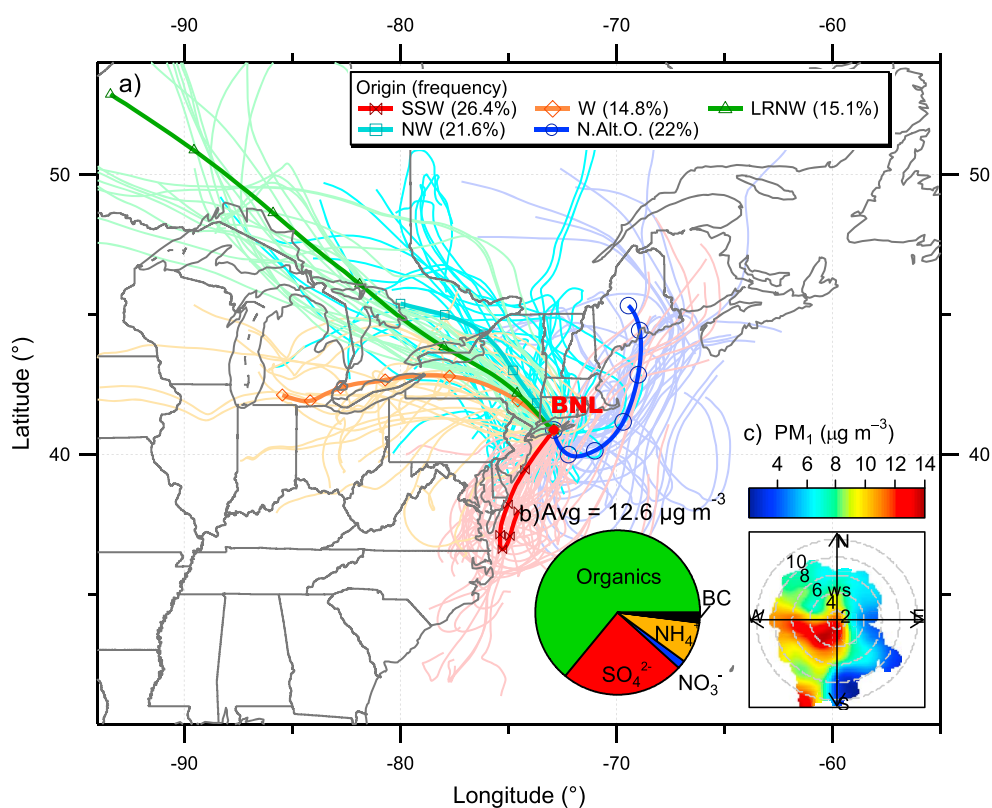


Figure 1. (a) Map of Long Island and East United States with the location of the sampling site (BNL). Seventy-two-hour back trajectories of air masses arriving at BNL every 3 h are shown on the map in light colors representing five clusters determined using the inbuilt function of the HYSPLIT software. Mean back trajectories of each cluster are shown in dark colors with markers indicating 12 h intervals. Cluster 1 circulating along the south-southwest with some passing over Philadelphia and Washington metropolitan areas (SSW, 26.4% of all trajectories), cluster 2 from the west passing over NYC metropolitan area (W, 14.8%), cluster 3 relatively long-range transported from the northwest Canadian forest (LRNW, 15.1%), cluster 4 from northwest (NW, 21.6%), and cluster 5 from the North Atlantic Ocean (N.Atl.O., 22%). (b) Average composition of PM₁ for the entire study period. (c) Bivariate polar plot of PM₁ concentration as a function of wind speed (m/s) and direction.

particle loss calculator by *von der Weiden et al.* [2009], the transmission efficiency ranges from ~95.5% to ~99.5% for particles with a diameter range of 30 nm–1 μm. The TD follows the design by *Fierz et al.* [2007] with a heated adsorption section. Aerosol residence time in the TD is 10 s at the experimental flow rate (0.9 L min⁻¹). The transmission efficiency of TD is ~90% based on the HR-AMS aerosol data at room temperature and at 30°C.

In addition, an extensive instrument suite was housed in two 6 m mobile laboratories, which are referred to as the Mobile Aerosol Observing Systems (MAOS; <https://www.arm.gov/sites/amf/mobile-aos>). The instrument suite contained in MAOS-A (for aerosol) provides measurements of aerosol optical properties, microphysical properties and composition, and black carbon (BC) mass through a Single Particle Soot Photometer (Droplet Measurement Technologies) [Sedlacek et al., 2012]. The instrument suite inside MAOS-C (for chemistry) is primarily focused on measurements of gaseous species including CO, CO₂, CH₄, NO_x, O₃, as well as volatile organic compounds (VOCs) using a high-resolution time-of-flight proton transfer reaction mass spectrometer (PTR-TOF-MS; Ionicon). Anions and cations in aerosols for daytime hours are also determined in MAOS-C. The instruments deployed in the MAOS are listed in Table S1 in the supporting information. An overview of these and other DOE Atmospheric Radiation Measurement (ARM) instrumentation can be found in *Mather and Voyles* [2013].

2.2. HR-AMS Operation and Data Processing

The HR-AMS was deployed downstream of the TD with an automated switching valve allowed for the sampling of aerosols under ambient bypass (BP) conditions or after being processed by the TD. The TD was operated at 12 temperatures, 10 min at each temperature, following the sequence of 30, 50, 70, 100, 150, 200, 180,

130, 110, 86, 66, and 40°C, which resulted in a full temperature cycle lasting 120 min, while the HR-AMS was alternating between V and W modes, for high-sensitive and high-mass-resolution sampling, respectively [DeCarlo *et al.*, 2006]. The TD HR-AMS system was thus operated under four distinct configurations: V_BP, W_BP, V_TD, and W_TD, each at 2.5 min averaging, allowing for detailed and comprehensive characterization of the concentrations, mass-based size distributions, and volatility profiles of NR-PM₁ species. HR-AMS was calibrated for ionization efficiency and particle sizing at the beginning and in the middle of this field campaign following standard protocols [DeCarlo *et al.*, 2006]. The 2.5 min detection limits of the five NR-PM₁ species (organics, sulfate, nitrate, ammonium, and chloride) were determined as 3 times the standard deviations (3σ) of the corresponding signals in particle-free ambient air and were 61.5, 9.4, 4.6, 3.8, and 8.1 ng/m³, respectively.

All HR-AMS data were processed using standard HR-AMS data analysis software, SQUIRREL v1.53 and PIKA v1.12. Default relative ionization efficiency (RIE) values were assumed for organics (1.4), nitrate (1.1), and chloride (1.3), while an RIE value of 3.3 was determined for ammonium and 1.4 for sulfate following the analysis of pure NH₄NO₃ and (NH₄)₂SO₄, respectively. The reported mass concentrations and size distributions of NR-PM₁ species corresponded to V-mode acquisition periods, while the high-resolution mass spectra (HRMS) and thus the elemental composition of OA were determined from W mode. Elemental ratios, such as atomic oxygen-to-carbon ratio (O/C) and hydrogen-to-carbon ratio (H/C), and organic mass-to-carbon ratio (OM/OC), were determined by following the latest procedures using the Improved-Ambient (IA) method [Canagaratna *et al.*, 2015]. Figure S1 in the supporting information compares the time-variation of elemental ratios determined from the IA method and the previously published Aiken-Ambient (AA) method [Aiken *et al.*, 2008]. The O/C, H/C, and OM/OC values determined from the two methods correlate tightly ($r > 0.98$), and those from the IA method were 14%, 16%, and 13%, respectively, larger than those based on the AA method. Results from both methods are reported here for comparison with literature results.

A Nafion dryer was placed upstream of the TD HR-AMS to eliminate potential RH effect on particle collection efficiency (CE) at the vaporizer [Middlebrook *et al.*, 2012]. A CE value of 0.5 was used for all data and validated by extensive intercomparison among HR-AMS and other collocated aerosol measurements. As shown in Figure S2, HR-AMS results correlated tightly with those of SMPS, aerosol chemical speciation monitor, and particle-into-liquid sampler coupled with ion chromatograph (PILS-IC), with Pearson's r values of 0.68–0.96 (see Text S1 in the supporting information for additional details). Note that HR-AMS on average reported only ~33% of the nitrate, and a few percent of the chloride measured by PILS-IC and the correlations between the HR-AMS and PILS measurements were low ($r = 0.63$ and 0.43 for nitrate and chloride, respectively). This was possibly because the HR-AMS primarily measures NR nitrate and chloride (e.g., NH₄NO₃ and NH₄Cl) and is insensitive to refractory species such as NaCl, KCl, and NaNO₃ at its vaporizer temperature of 600°C, while PILS-IC is able to measure both NR and refractory inorganic species. Given the proximity of BNL to the Atlantic Ocean, sea salt was likely a significant contributor to fine PM. Indeed, PILS-IC observed elevated Na⁺ concentrations and evidence for chloride depletion in PM_{2.5} (Figure S3), indicating the presence of aged sea-salt particles. However, almost no NaCl⁺ ($m/z = 57.9586$) signal was detected in the HR-AMS spectra during this study.

2.3. Positive Matrix Factorization of Organic Aerosol Matrix

Positive Matrix Factorization (PMF) was performed on the HRMS of organics using the PMF2 algorithm (v4.2) in robust mode [Paatero and Tapper, 1994]. The ion-specified HRMS matrix and the corresponding error matrix were first generated from PIKA, and then analyzed using the PMF Evaluation Tool v2.05 [Ulbrich *et al.*, 2009]. The OA data and error matrices were refined prior to PMF analysis according to the protocol summarized previously [Ulbrich *et al.*, 2009; Zhang *et al.*, 2011]. Details of data pretreatment and results evaluation are included in Text S2. In this study, the three-factor solution with $f_{\text{Peak}} = 0$ ($Q/Q_{\text{expected}} = 0.99$) was selected as the optimum solution. Key diagnostic information for this PMF solution can be found in Figure S5. The average size distribution of OA factors and their temporal variations at different TD temperatures were then derived using linear decomposition based on the method described in Ge *et al.* [2012a]. Additional details are given in Text S3.

2.4. Air Mass Trajectory Analysis and Classification

The Hybrid Single-Particle Lagrangian Integrated Trajectory (HYSPPLIT) model [Draxler and Hess, 1998] with meteorology input from NOAA Air Resource Laboratory Archived Eta Data Assimilation System (EDAS40)

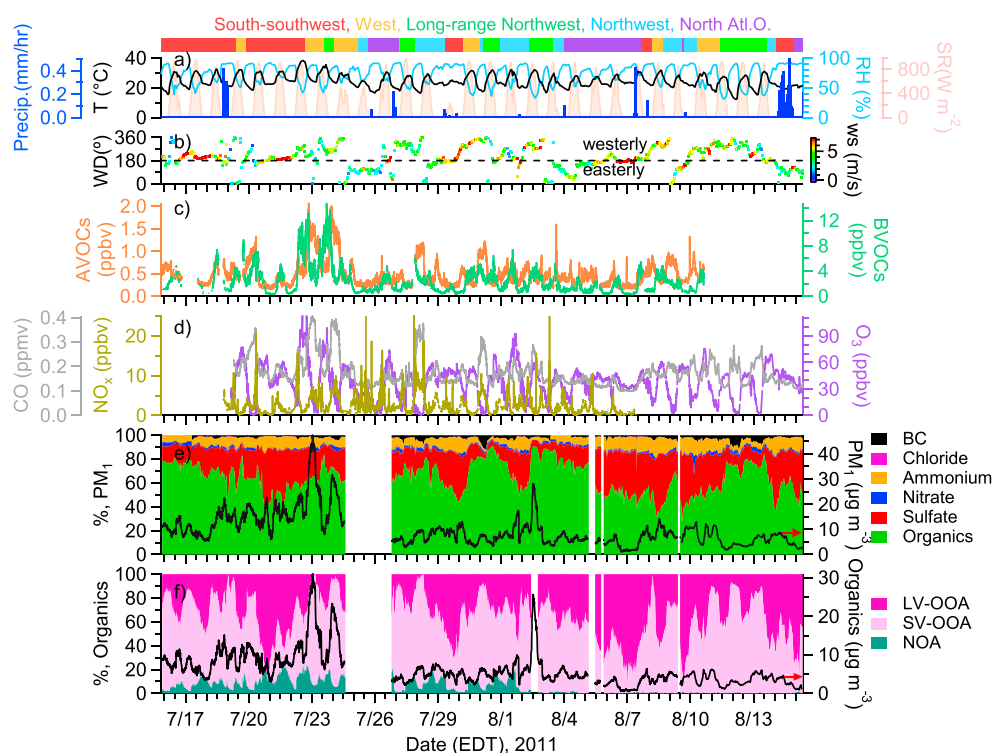


Figure 2. Time series of (a) meteorological variables such as hourly precipitation (Precip), temperature (T), relative humidity (RH), and broadband solar radiation (SR); (b) hourly wind direction colored by wind speed; (c) mixing ratios of total anthropogenic VOCs (=benzene + toluene + xylene), and total biogenic VOCs (=isoprene + MVK + MCAR + monoterpenes + sesquiterpenes); (d) mixing ratios of CO, NO_x, and O₃; (e) percentage contribution of the species to the total PM₁ mass; and (f) percentage contribution of OA factors to total OA mass (missing OA factor data on 2 August was due to the removal of a transported wildfire plume episode prior to PMF analysis). The color bars shown on the top indicate air mass origins based on cluster analysis of back trajectories (see Figure 1).

(<http://ready.arl.noaa.gov/HYSPLIT.php>) was used to investigate the influence of air mass origin on ambient aerosol characteristics. Three-day backward trajectories of air masses arriving at BNL and initialized at 50 m above ground level were calculated every hour for the entire campaign period resulting in 744 calculated trajectories. Clustering-based spatial distribution of the back trajectories was performed using the built-in function of the HYSPLIT software with an optimum solution of five clusters, as shown in Figure 1a.

2.5. Bivariate Polar Plots

Bivariate polar plots were calculated using the OpenAir software [Carslaw, 2015; Carslaw and Ropkins, 2012] to explore potential source regions for various gaseous and particulate species. The wind data used in these plots were measured from the met tower at BNL at a height of 85 m above ground level rather than at the surface as the latter was more influenced by surrounding conditions. As shown in Figure 1c, higher concentrations of PM₁ were associated with high wind speeds from the west and southwest, suggesting that highly urbanized areas are the source of transported PM at BNL.

3. Results and Discussion

3.1. Overview of PM₁ Composition, Size Distribution, and Temporal Characteristics

3.1.1. Concentration and Composition of PM₁

Figure 2 presents an overview of the meteorological conditions and concentrations of gas-phase species and PM₁ species at BNL from 15 July to 15 August 2011. The weather during this campaign was relatively hot (average $T = 24.4 \pm 4.3^\circ\text{C}$) and humid (average $\text{RH} = 73.9 \pm 15.5\%$), with intermittent rain (Figure 2a). VOC composition measured by PTR-ToF-MS indicates that BNL was highly influenced by biogenic emissions (Figure 2c). The average concentration of total biogenic VOCs (BVOCs = isoprene + MVK/MCAR + monoterpenes + sesquiterpenes) was 2.4 ppbv, about 5 times the average concentration (0.50 ppbv) of

anthropogenic VOCs (AVOCs = benzene + toluene + xylene). Note that previous studies indicated that toluene can be emitted from biogenic sources as well and show good correlation with α -pinene [Heiden *et al.*, 1999; White *et al.*, 2009]. In this study, we also observed a good correlation between toluene and monoterpene ($r^2 = 0.62$; Figure S7c). However, the diurnal profile of toluene exhibited a morning peak at $\sim 7:30$ A.M., so did those of anthropogenic tracers such as benzene, xylene, CO, and BC. In contrast, monoterpene did not show an increase in the morning (Figure 5). Furthermore, toluene correlated better with benzene ($r^2 = 0.75$; Figure S7a) and xylene ($r^2 = 0.79$; Figure S7b) than with monoterpene ($r^2 = 0.62$; Figure S7c). These results suggest that although biogenic emissions could have influenced toluene concentrations during this study, anthropogenic sources seem to be a more important contributor.

PM₁ varied dynamically with the 2.5 min average concentration ranging from 1.2 to 47.5 $\mu\text{g m}^{-3}$ (Figure 2e) with generally higher PM₁ loading from 15 July to 25 July, when BNL was primarily influenced by airflow from the west and south-southwest (Figure 2). Meir *et al.* [2013] reported that during 22–24 July 2011 an extreme heat event impacting NYC caused Urban Heat Island (UHI) effect and deflected the southerly sea breeze eastward, which brought urban pollution to its outskirts. The significant enhancement of PM loading at BNL, as well as the total anthropogenic VOCs (AVOCs = benzene + toluene + xylene), CO, and NO_x, in the evenings of 22 July and 23 July were likely associated with this UHI event in NYC. Another event with elevated PM₁ concentration up to $\sim 28 \mu\text{g m}^{-3}$ was observed on 2 August 2011, due to the influence of transported wildfire plumes from Canada [Sedlacek *et al.*, 2012]. Biomass burning tracers, HR-AMS f_{60} ($=\text{C}_2\text{H}_4\text{O}_2^+ (m/z 60)/\text{OA}$), and acetonitrile concentrations all increased during this event (not shown). Note that this plume appeared to be highly diluted as CO mixing ratios were not significantly elevated and BC accounted for only $\sim 1.3\%$ to the total PM₁ mass.

The average concentration of PM₁ (=sulfate + ammonium + nitrate + organics + chloride + BC) was 12.6 $\mu\text{g m}^{-3}$. Organics frequently dominated PM₁ mass with an average contribution of 64.0%, followed by sulfate (24.2%), ammonium (8.1%), nitrate (1.6%), and BC (1.9%; Figure 1b). The dominance of organics and sulfate in PM₁ was similar to previous observations at NYC in summertime [Drewnick *et al.*, 2004b; Sun *et al.*, 2011]. The stoichiometric neutralization for NR-PM₁ was examined by comparing the ammonium concentrations measured by HR-AMS to those needed to fully neutralize the AMS-measured concentrations of anionic species, i.e., sulfate, nitrate, and chloride [Zhang *et al.*, 2007]. Particles appeared to be on average neutralized with a few plumes indicating moderately acidic aerosols (Figure S8a).

There are indications that a significant fraction of the nitrate measured by HR-AMS at BNL was attributed to organonitrate. The average ratio of the signals for the two largest nitrate fragments, NO⁺ ($m/z = 30$) and NO₂⁺ ($m/z = 46$), was 3.94 during the campaign (Figure S8b), substantially higher than the NO⁺/NO₂⁺ ratio measured for pure ammonium nitrate particles (R_{AN}) during this study (1.83). Previous studies reported that the ratio for organonitrates (R_{ON}) can be 2–4 times higher than for NH₄NO₃ [Alfarra *et al.*, 2006; Fry *et al.*, 2009, 2013]. In addition, significant amounts of ion fragments from the C_xH_yO_zN_p⁺ family were unambiguously observed in the HRMS, providing further evidence for the presence of organonitrates [Fry *et al.*, 2013; Rollins *et al.*, 2010]. Assuming that the ratio of the ratios ($R_{\text{ON}}/R_{\text{AN}}$) is stable, based on equation (1) in Farmer *et al.* [2010], we estimated that 67%–95% of the nitrate mass observed at BNL can be attributed to organonitrate. The presence of organosulfate is also confirmed based on the unambiguous detection of methanesulfonic acid (MSA) signature ions, i.e., CH₂SO₂⁺, CH₃SO₂⁺, and CH₄SO₃⁺, and their ratios in the HR-AMS spectrum. These three ions correlated well with each other, and their signal intensity ratios (CH₂SO₂⁺/CH₃SO₂⁺ = 0.31; CH₄SO₃⁺/CH₃SO₂⁺ = 0.34; Figure S9) were close to those observed in the HR-AMS spectrum of pure methanesulfonic acid [Ge *et al.*, 2012b], indicating the presence of mesylate (CH₃SO₃⁻, the deprotonated anion of MSA) in aerosol sampled during the study. We estimated the MSA concentration ($m\text{MSA}$) using the following equation:

$$m\text{MSA} = m\text{CH}_3\text{SO}_2^+ / 0.087 \quad (1)$$

where $m\text{CH}_3\text{SO}_2^+$ is the organic-equivalent concentration of CH₃SO₂⁺ ($\mu\text{g m}^{-3}$) and 0.087 is its fractional contribution to the total signal in the HR-AMS spectrum of pure MSA [Ge *et al.*, 2012b]. The average ($\pm 1\sigma$) MSA concentrations were $0.66 \pm 0.45 \mu\text{g m}^{-3}$ during this study.

3.1.2. Size-Resolved Aerosol Composition

The campaign-averaged size distributions of NR-PM₁ species and size-resolved aerosol composition are shown in Figure 3. All species showed an overlapping accumulation mode peaking at ~ 500 nm (D_{va}), which

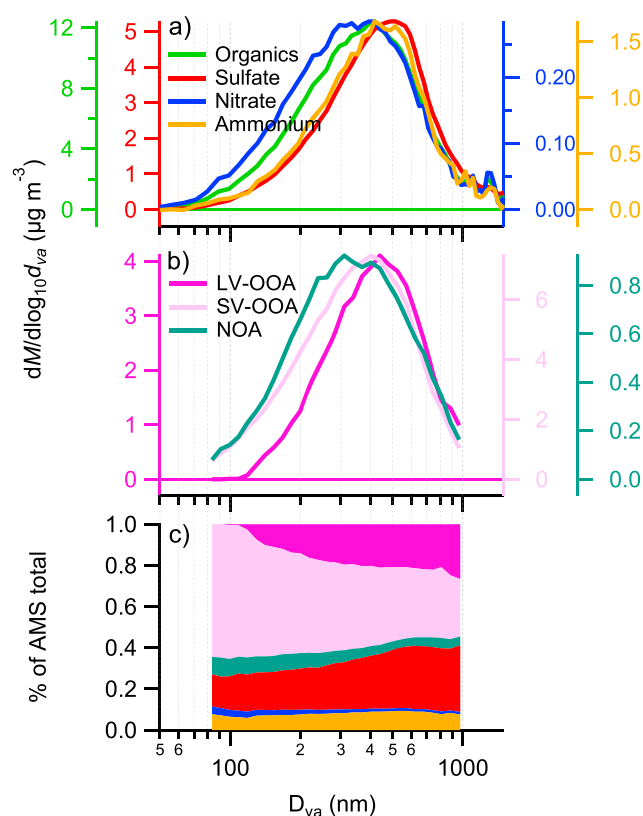


Figure 3. Average size distributions of (a) HR-AMS species, (b) OA factors, and (c) size resolved mass fractional composition of NR-PM₁. The size distribution of chloride is not included here due to its low signal-to-noise.

was indicative of internally mixed regional particles. Very similar size distributions of secondary aerosol species such as sulfate and OOA were observed previously in the Northeastern U.S. such as Pittsburgh [Zhang *et al.*, 2005a, 2005b] and NYC [Drewnick *et al.*, 2004a; Sun *et al.*, 2011]. Given the humid weather during the campaign, where RH was frequently above 90% at night (Figure 5), aqueous phase processing likely played a significant role in the formation of sulfate and OOA (more discussions are given in section 3.2.2). Both nitrate and organics exhibited a second condensational mode extending to smaller sizes below 200 nm, suggestive of formation and growth of these two species by gas-to-particle partitioning. The lack of a prominent Aitken mode for organics indicates that fresh vehicular emissions did not make a significant contribution to the observed aerosol concentration and composition, which is consistent with the rural nature of BNL.

3.1.3. Bulk Chemical Composition and Elemental Ratios of OA

Consistent with its size distribution suggestive of an aged origin, organics were overall oxidized with an average

O/C = 0.62 (0.45–1.04) and OM/OC = 1.97 (1.78–2.50) calculated with the IA method (Figure 4). O/C derived from the AA method was 0.47 (0.35–0.76). The comparison between elemental ratios determined from the IA and AA methods is discussed in section 2.2. In the average HRMS of organics (Figure 4a), hydrocarbon ions ($C_xH_y^+$) together accounted for only 36% of the total OA signal and the peak at m/z 57 contributed only 1.2%. m/z 57 is a prominent peak composed nearly completely of $C_4H_9^+$ in the mass spectra of POA from vehicle emissions [Collier *et al.*, 2015] and has been used as an AMS spectral tracer for hydrocarbon-like OA (HOA) in urban environments. However, at BNL, the m/z 57 signal was mainly contributed by an oxygenated ion— $C_3H_5O^+$ (62.7%), while only 24.2% was associated with $C_4H_9^+$. These results indicate that traffic-related POA was a minor component of the OA sampled at BNL.

A notable amount of nitrogen-containing organic compounds was present in particles at BNL, as indicated by the unambiguous detection of $C_xH_yN_p^+$ and $C_xH_yO_zN_p^+$ ions, most notably $C_3H_8N^+$, CH_4N^+ , $C_2H_4N^+$, and $CHNO^+$ (Figure 4c). As shown in Figure 4a, the average nitrogen-to-carbon (N/C) ratio of OA was 0.025. Periods with much higher N/C ratios (0.05–0.07) were observed before 1 August, and a sudden decrease occurred after that with a sharp decrease of signals from fragments characteristic of reduced amines (Figure S10a). As discussed in more detail in section 3.2.3, a possible reason for this sharp decrease was change of emission.

3.1.4. Diurnal Cycles

The average weekday (Monday–Friday) and weekend (Saturday–Sunday) diurnal profiles for PM₁ species, several trace gases, and meteorological variables are presented in Figure 5 to provide insight into the emission sources and atmospheric processing dynamics of air pollutants at BNL. The diurnal variations in meteorological conditions did not change significantly from the weekdays to the weekends, except that more rain occurred during the weekends of this study. In addition, as expected, the weekday and weekend diurnal profiles for terpenes (=monoterpenes + sesquiterpenes) were almost identical and both peaked during night

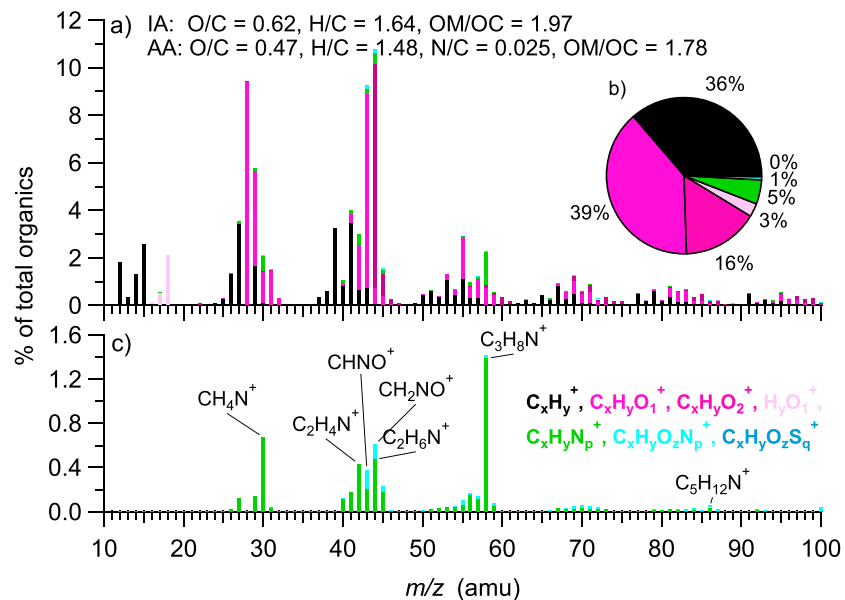


Figure 4. (a) Average OA spectrum, (b) average OA composition colored by the contributions of seven ion categories, and (c) average spectrum of all the nitrogen containing ions for the study period. The average elemental and OM/OC ratios of OA calculated using both Ambient-Aitken (AA) and Improved-Aitken (IA) methods are also shown in the legend of Figure 4a.

and dropped rapidly once the concentrations of oxidants (e.g., O_3) rose in the morning. The diurnal profiles of benzene, toluene, and xylene (i.e., AVOCs) were also similar between the weekdays and the weekends, but those of combustion tracer species such as BC, CO, and NO_x were clearly different with weekday profiles showing a distinct peak at ~8 A.M., likely due to increased traffic emissions during morning rush hours. The average weekday diurnal cycle of AVOCs, which have important emission sources from vehicle exhaust, demonstrated a small peak at ~8 A.M. as well. The average increases of BC, CO, NO_x , and AVOCs on weekdays between 5 and 8 A.M. were $\sim 0.11 \mu g m^{-3}$, ~ 20 ppbv, ~ 5 ppbv, and 0.05 ppbv, respectively (Figure 5), much

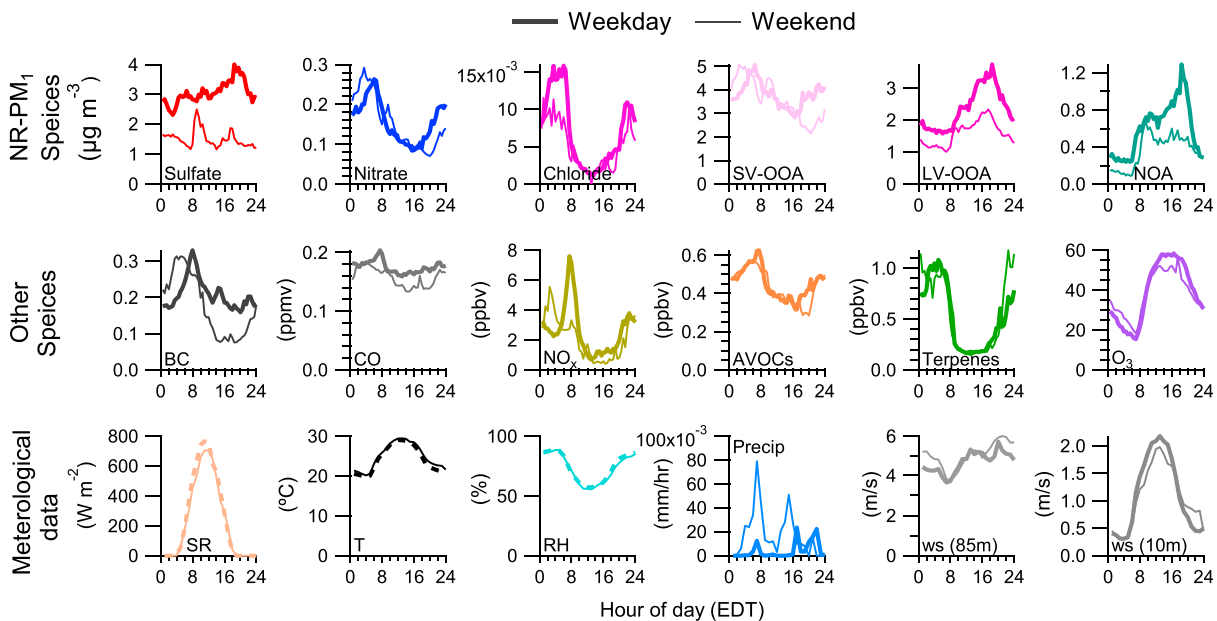


Figure 5. Average diurnal cycles of PM_{10} species, CO, NO_x , AVOCs (=benzene + toluene + xylene), terpenes (=monoterpenes + sesquiterpenes), and meteorological variables for weekdays and weekends during the campaign. Note that periods under the influence of NYC UHI effect (i.e., the evenings of 22 July and 23 July) were excluded in the average diurnal profiles.

lower than the increases typically seen during morning rush hours at urban locations [Gentner *et al.*, 2009; Lin *et al.*, 2012; Rattigan *et al.*, 2013; Young *et al.*, 2016; Zhang *et al.*, 2005a]. The relatively small increase in traffic emission tracers during morning rush hours at BNL is consistent with the rural setting of BNL and limited local habitation. In addition, given the distance between BNL and NYC (~80 km) and low wind speeds in early morning (4–5 m/s at 85 m and < 0.5 m/s at ground level; Figure 5), emissions from busy traffic near NYC were unlikely responsible for the morning peaks of primary air pollutants observed at BNL.

Nitrate, chloride, and semivolatile oxygenated organic aerosol (SV-OOA) all showed nighttime increases, which were primarily caused by gas-particle partitioning due to their semivolatile characteristics. The diurnal profiles of sulfate and low-volatility oxygenated OA (LV-OOA), on the other hand, showed an increase in late afternoon, likely due to photochemical production of secondary aerosol species. In addition, the concentrations of sulfate and LV-OOA were on average lower during the weekends compared to the weekdays, for which a possible reason is the difference in the prevailing wind directions, thus source regions, between weekdays and weekends. More discussions on OA factors and their diurnal patterns are given in section 3.2.

3.2. Organic Aerosol Sources and Processes

PMF analysis of HR-AMS data sets has proved to be a useful method for extracting distinct OA factors that are associated with different sources and atmospheric processes [Lanz *et al.*, 2007; Ulbrich *et al.*, 2009; Zhang *et al.*, 2011]. Our analysis of the HRMS of OA identified three factors, all of which were secondary in nature, as discussed below. Note that the period influenced by a transported BB plume event on 2 August was removed before PMF analysis due to the short duration of the plume as well as to avoid interferences on the determination of general profiles of aerosol sources during this study. Our inability to separate an HOA factor is consistent with the fact that $C_4H_9^+$ was a minor peak in the OA spectra and the average organic-equivalent concentration of $C_4H_9^+$ was only $0.018 \mu\text{g m}^{-3}$ during this study (Figure 5a). Collier *et al.* [2015] reported that the average $f_{C_4H_9^+}$ (fraction of total organic signal accounted for by $C_4H_9^+$) is 8.1% in the HRMS of POA from vehicle emissions. Based on this relationship and assuming all $C_4H_9^+$ signal came from HOA, we estimate an average HOA concentration of $0.22 \mu\text{g m}^{-3}$, which is 2.6% of the total OA mass measured at BNL. Note that this number was likely an upper bound estimate of HOA concentration since $C_4H_9^+$ can be found in the AMS spectra of other OA types. Indeed in this study, $C_4H_9^+$ was fit well in the PMF analysis with very small residual (Figure S5i) and was found to be mostly associated with SV-OOA and a nitrogen-enriched OA factor (NOA).

3.2.1. Semi-Volatile Oxygenated OA (SV-OOA) and Association With Transported Urban Emissions

SV-OOA dominated the OA composition, making up an average 63% of the OA mass during this study (Figure 6d). The semivolatile nature of SV-OOA was validated using the thermograms, which show that SV-OOA and nitrate had similar volatility profiles with ~50% mass loss at ~80°C (Figure 6e). The average mass spectrum of SV-OOA was characterized by a larger $C_2H_3O^+$ ($m/z = 43$) than CO_2^+ ($m/z = 44$; Figure 6b), similar to the SV-OOA spectrum observed previously at NYC in summer 2009 [Sun *et al.*, 2011]. SV-OOA was moderately oxidized, with an average O/C ratio of 0.54 calculated using the IA method (0.41 using the AA method), and within the range of O/C values of SV-OOA observed worldwide [Jimenez *et al.*, 2009; Ng *et al.*, 2010]. In addition, the temporal profile of SV-OOA correlated tightly with the time series of $C_xH_y^+$ and $C_xH_yO^+$ ions (Figure S11), suggesting that this factor was mainly composed of oxygenated compounds containing hydrocarbon moieties.

The correlations of the time series of the OA factors and other aerosol and gas phase species were examined, and the Pearson's r values are summarized in Table S1. SV-OOA and nitrate exhibited a tight correlation ($r = 0.92$; Figure 6g) and both showed clear diurnal patterns with elevated concentrations at night (Figure 6j). SV-OOA also exhibited fairly good correlations with CO and BC, tracers for combustion emissions ($r = 0.85$ and 0.72 , respectively; Figure 6g), and with VOCs with an important emission source from vehicle exhaust (e.g., benzene, toluene, and xylene; $r = 0.78$, 0.80 , and 0.80 , respectively; Figure 6g and Table S1). However, unlike those of the primary pollutants, the average diurnal profiles of nitrate and SV-OOA were fairly similar between the weekdays and the weekends except that only the weekday profiles demonstrated a small peak between 6–7 A.M. (Figure 5). In addition to air temperature and RH, boundary layer dynamics might have played a significant role in driving the diurnal behaviors of SV-OOA and nitrate as well. For example, surface ozone concentration demonstrated a rapid increase starting around 6–7 A.M. (Figure 5), suggesting downward mixing of pollutants from the aloft residual layer [Zhang and Rao, 1999]. A general mechanism for residual layer formation is the collapse of the boundary layer at sunset, which leads to the decoupling of pollutants that mixed aloft during the day from the surface. The residual layer above BNL was likely enriched of urban pollutants since

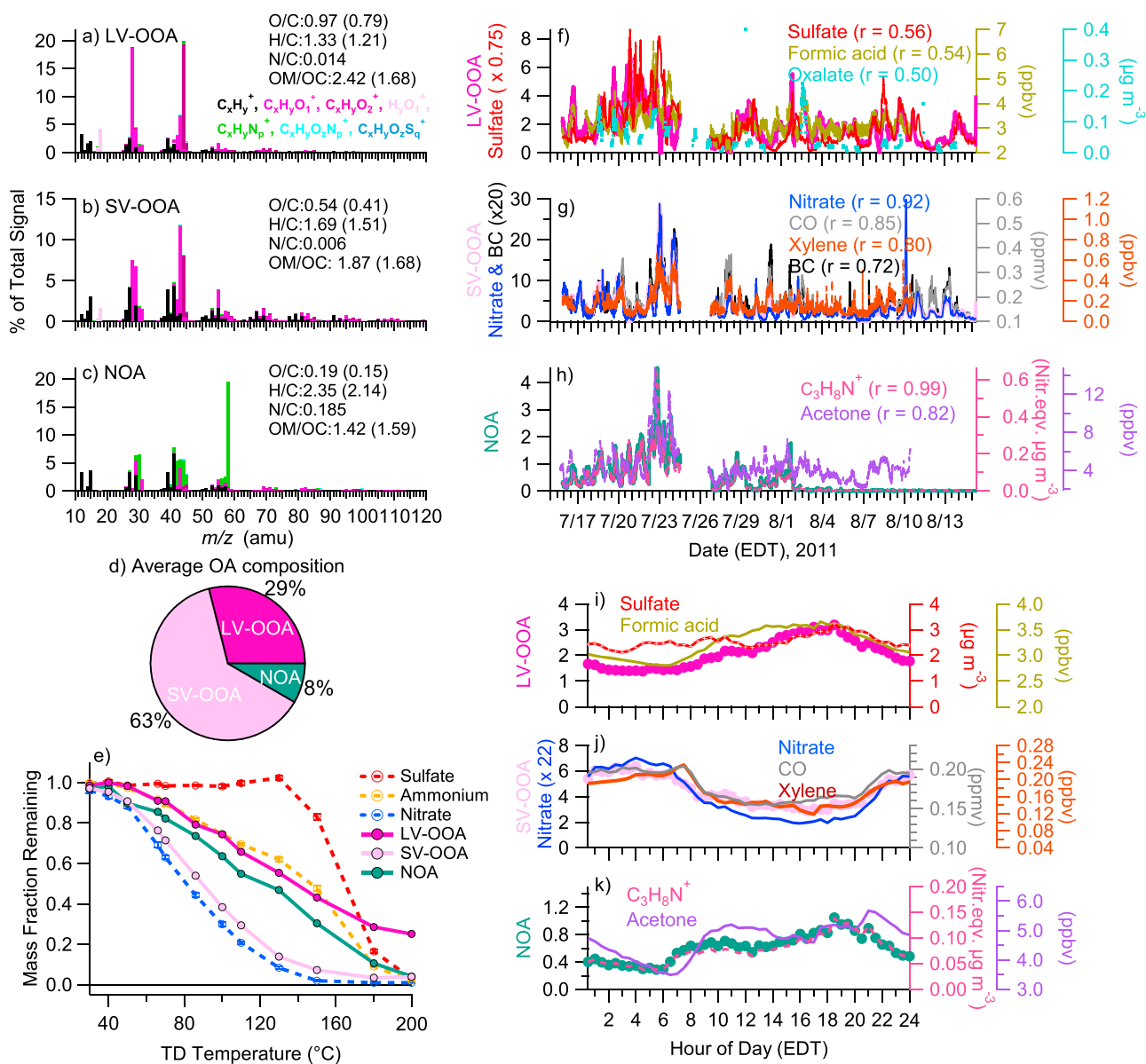


Figure 6. (a–c) HRMS of individual OA factors colored by seven ion categories. (d) A pie chart of the average mass distribution of the three OA factors during the entire study. (e) The volatility profiles for the main HR-AMS species and the OA factors. (f–h) The time series of the OA factors and the corresponding tracer compounds. Note that the *r* between NOA and acetone reported in (h) is for high-NOA period (15 July to 1 August) only. (i–k) The diurnal patterns of the OA factors and their respective tracers. The elemental ratios of each factor calculated with the IA method are shown in the legends of Figures 6a–6c with those obtained using the AA method in parenthesis.

emissions from NYMA were advected continuously with the synoptic westerly winds. As the boundary layer evolved in the morning, tracers for urban emissions, as well as secondary species formed through nighttime chemistry (e.g., nitrate and SV-OOA), got rapidly entrained into the mixing layer and contributed to the increase in the ground-level concentrations. Further growth of the mixing layer led to a stronger dilution and a decrease in the concentrations of transported pollutants, while ozone continued to build up from photochemical production.

In order to further evaluate the hypothesis that advection of urban emissions significantly influenced air quality at BNL, we examine the concentrations of aerosol species and gas phase pollutants as a function of wind speed and direction using bivariate polar plots (Figure 7). Several interesting features can be seen in the polar plot of SV-OOA concentration. First, the highest concentration occurred under relatively low wind speed

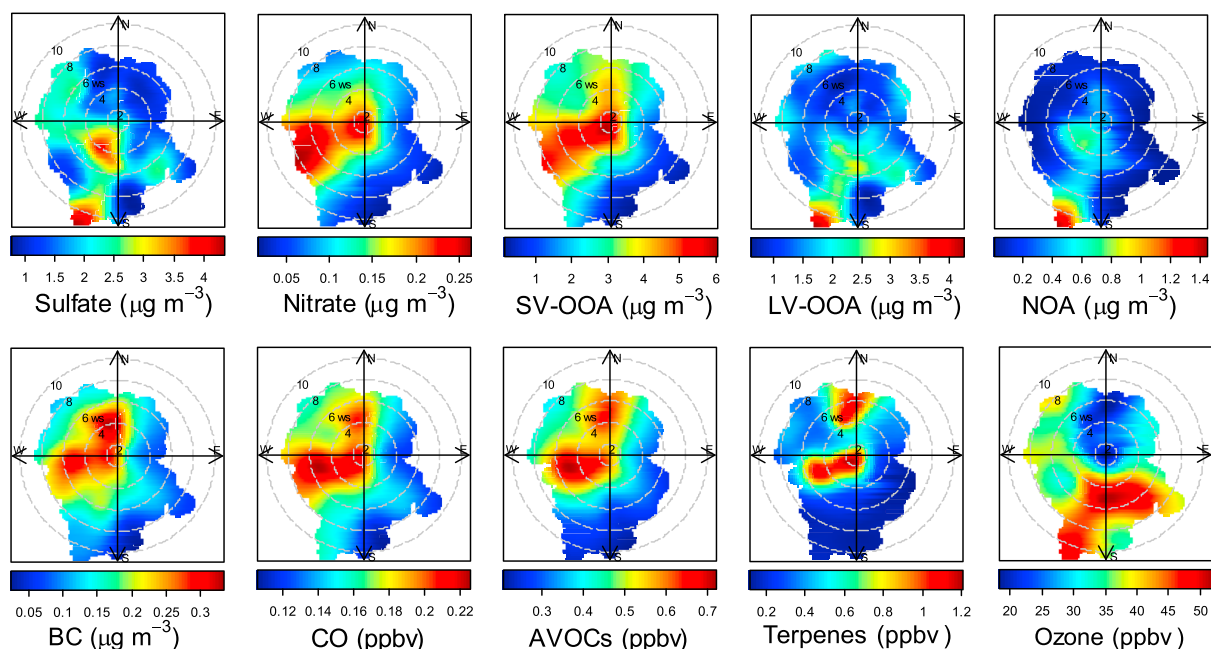


Figure 7. Bivariate polar plots of aerosol and gas phase pollutants as a function of wind speed (m/s) and direction.

(<3 m/s) conditions, which is suggestive of local formation of SV-OOA. Second, higher concentrations of SV-OOA were also associated with airflow from the west and southwest, where most of the metropolitan areas lie. This is an indication that continuous advection, especially when winds were from the W-SW, also led to high SV-OOA observed at BNL. Similar features were observed for nitrate, BC, CO, and AVOCs (Figure 7), where the highest concentrations were observed to the west-southwest at higher wind speeds (4–6 m/s). In addition, the highest concentration of BC and above-average concentration of SV-OOA, CO, and AVOCs were also observed under the influence of high-speed northern winds. These results corroborate the hypothesis that emissions from the heavily urbanized northeast megalopolis region, including NYC and New Jersey to the W and SW of BNL and cities in Connecticut and Massachusetts to the N, significantly influenced aerosol loading and composition at Long Island.

3.2.2. Low-Volatility Oxygenated OA (LV-OOA) and Association With Aqueous Phase Processing

LV-OOA represented 29% of the total OA mass (Figure 6d) and has a mass spectrum (Figure 6a) that was characterized by a dominant peak at $m/z = 44$ (CO_2^+ ; 18.7% of the total LV-OOA signal), a high O/C ratio (0.97 calculated with the IA method; 0.79 with AA method), and a low H/C ratio of (1.33 and 1.21 with IA and AA method, respectively). According to the thermograms shown in Figure 6e, LV-OOA was the least volatile OA factor and much less volatile than nitrate. In addition, although LV-OOA was on average more volatile than sulfate at TD temperature less than 180°C , over 20% of LV-OOA mass remained in the particle phase above this temperature, suggesting that it contained a significant fraction of extremely low-volatility organic compounds (ELVOC). A possible source of these compounds is gas phase oxidation of α -pinene and isoprene, which were reported to produce highly oxidized multifunctional compounds with very low volatilities [Ehn *et al.*, 2014; Jokinen *et al.*, 2015]. In addition, aqueous-phase photochemistry has also been proposed to be an important pathway for the formation of low volatility, higher molecular weight oligomer products [Ervens *et al.*, 2011], and a large number of highly oxidized ELVOCs were indeed observed during the aqueous-phase oxidation of phenolic compounds [Yu *et al.*, 2016].

LV-OOA correlated with sulfate and ozone ($r = 0.56$ and 0.60 , respectively, Figure 6f and Table S1) and showed similar polar plot features with higher concentrations from S and SW at high wind speed (Figure 7). These observations suggest a more regional source of LV-OOA. In addition, the correlations between LV-OOA and organic ions such as acetate, oxalate, and gas phase formic acid ($r = 0.58$, 0.50 , and 0.54 respectively, Figure 6f and Table S1) further suggest that the LV-OOA observed at BNL was likely influenced by aqueous-phase processing. For instance, aqueous-phase oxidation is an important production pathway for organic acids, and oxalic acid, in particular, has a significant source from fog/cloud processing

[Sorooshian *et al.*, 2006; Yu *et al.*, 2005]. The LV-OOA mass spectrum, characterized by abundant CO_2^+ (Figure 6a) and HCO_2^+ ions, suggests a relatively high mass fraction of carboxylic functional groups and thus a significant contribution from carboxylic acids to LV-OOA composition. In addition, the size distribution of LV-OOA and sulfate were highly similar and both exhibited narrow profiles with a droplet mode peaking at ~ 500 nm (Figure 3b), which was similar to the size distributions of secondary aerosol species subjected to aqueous-phase reactions [e.g., Ge *et al.*, 2012b]. Furthermore, HYSPLIT back trajectory analysis of the air masses arriving at BNL on 21 July indicates that RH reached 100% along its trajectories, suggesting the occurrence of aqueous-phase processes during transport. On this day, NR-PM₁ composition was dominated by sulfate and LV-OOA with LV-OOA accounting for $\sim 80\%$ of total OA mass (Figure 2). These observations suggest that an aqueous production route likely contributed to the LV-OOA observed at BNL.

3.2.3. Nitrogen-Enriched OA (NOA) and Association With Industrial Amine Emissions

In addition to SV-OOA and LV-OOA, a nitrogen-enriched OA (NOA; N/C = 0.185) factor was identified in this study, and it accounted for 8% of the total OA mass (Figure 6d). The mass spectrum of NOA (Figure 6c) was characterized by a dominant peak at m/z 58 (mostly $\text{C}_3\text{H}_8\text{N}^+$), which is a dominant ion in the HR-AMS MS of trimethylamine and diethylamine (Ge *et al.*, in preparation). Other prominent mass spectral fragments included CH_4N^+ ($m/z = 30$), $\text{C}_2\text{H}_4\text{N}^+$ ($m/z = 42$), $\text{C}_2\text{H}_6\text{N}^+$ ($m/z = 44$), and $\text{C}_5\text{H}_{12}\text{N}^+$ ($m/z = 86$), which are typically representative of aliphatic amines ($\text{C}_n\text{H}_{2n+2}\text{N}^+$). Fragments representative of amides ($\text{C}_x\text{H}_y\text{NO}^+$), e.g., CHNO^+ ($m/z = 43$) and CH_2NO^+ ($m/z = 44$), were also observed. NOA has a relative low degree of oxidation (O/C = 0.19 and 0.15, respectively, according to the IA and AA methods) and a high fraction (44.2%) of $\text{C}_x\text{H}_y\text{N}_p^+$ signals.

In this study, the NOA concentration varied dynamically before 1 August, but suddenly became very small afterward (Figure 6k). According to the polar plot (Figure 7), higher concentrations of NOA occurred under high SW wind conditions, suggesting its association with emissions from that direction. A similar NOA factor was identified in NYC in summer 2009 [Sun *et al.*, 2011, 2012a], and it had a similar potential source region (south of NYC). Furthermore, we observed a fairly good correlation between NOA and acetone—a frequently used industrial organic solvent, especially for the high-NOA period before 1 August ($r = 0.82$). These observations together suggest that NOA might be associated with emissions from industrial processes and that the sudden reduction of the air concentrations of NOA after 1 August could be explained by the interruption of certain manufacturing activities.

Previous studies indicate that amines can be directly emitted into the atmosphere through various industrial processes [Ge *et al.*, 2011; Zheng *et al.*, 2015]. Formation of amine salts can occur through reactions of amino compounds with acid gases and displacement of ammonium in both ammonium nitrate and ammonium sulfate [Lloyd *et al.*, 2009; Murphy *et al.*, 2007]. For the high-NOA period, NOA correlated with sulfate ($r = 0.69$), formic acid ($r = 0.74$), and acetic acid ($r = 0.62$; Table S1). In addition, the size distribution of NOA peaked at a condensation mode ($D_{va} \sim 200\text{--}300$ nm; Figure 3b). These results together suggest that acid-base reactions of amino compounds with acid gases likely have led to the production of amine salts followed by condensation onto the existing particles. NOA overall, as shown in Figure 6d, was slightly more volatile than LV-OOA and ammonium sulfate, but was much less volatile than ammonium nitrate and SV-OOA, consistent with the volatility of aminium salts formed by combining a series of amines with acetic and propanoic acid in the laboratory [Smith *et al.*, 2010]. Furthermore, the diurnal patterns of NOA (Figure 6k) showed a clear trend increasing gradually from morning and peaking in the late afternoon, likely due to daytime photochemical production of gas phase acids.

3.3. Influence of Air Mass Origins on Aerosol Characteristics at BNL and Indications of Enhanced SOA Formation in Mixed Urban Plumes and Biogenic Emissions

In order to investigate how upwind emissions affect aerosol characteristics at BNL, we examined the association of particle concentration and composition with air mass origins determined via cluster analysis of HYSPLIT back trajectories. As shown in Figure 8, aerosol characteristics were significantly different for different emission regimes. For example, PM₁ concentrations were generally lower when Long Island was under the influence of air masses from remote areas such as the North Atlantic Ocean and Canadian Forest in the NW, with measured mass concentrations only about half of those during periods of continental and coastal air mass influence. Aerosols associated with oceanic emissions were largely free from anthropogenic influences and appeared to be aged. We observed high contributions of sulfate and LV-OOA to PM₁ mass concentration in air masses coming from the ocean, while AVOCs and CO concentrations were the lowest in this cluster.

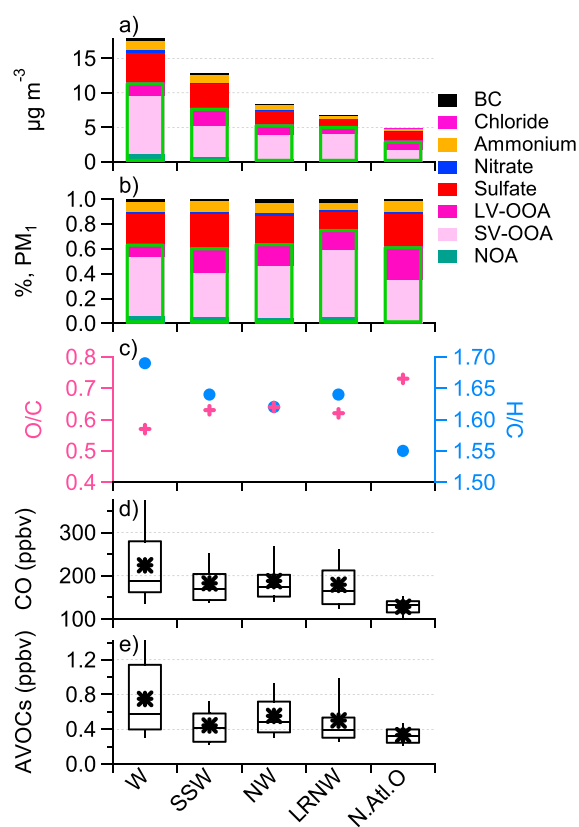


Figure 8. (a) Stacked average concentrations and (b) mass fractional contribution of PM_{10} species, (c) the average O/C and H/C of organic aerosols, (d) CO, and (e) AVOCs mixing ratios for each air mass cluster. The mean back trajectory and corresponding time periods for each cluster are in Figures 1 and 3, respectively. The box and whisker plots show the median (line), mean (star), upper and lower quartiles (box), and 10th and 90th percentiles (whiskers).

As shown in Figure 9, BNL had much higher biogenic emissions and substantially lower anthropogenic emissions compared to NYC. Isoprene mixing ratio was on average 1.02 ppbv, ~ 3.3 times higher than that observed at NYC (0.31 ppbv). The polar plot of the mixing ratio of terpenes at BNL (Figure 7) demonstrates that the highest concentrations occurred under relatively low wind speed (<3 m/s), which is suggestive of substantial local emissions of terpenes, consistent with the known biome surrounding of BNL (pine-oak forest). Meanwhile, anthropogenic VOCs, such as benzene, toluene, and xylene, and particulate species from urban primary emissions (e.g., HOA, COA, and BC) were in substantially lower concentrations at BNL. For example, average benzene concentration was 0.1 and 0.17 ppb for BNL and NYC respectively, while average BC concentration was $0.22 \mu\text{g m}^{-3}$ at BNL and $0.7 \mu\text{g m}^{-3}$ at NYC. Nitrate, an anthropogenic secondary species, was also much lower at BNL (Figure 9).

It is interesting to note that sulfate concentration was comparable at both sites with an average concentration of $\sim 2.8 \mu\text{g m}^{-3}$. LV-OOA concentrations were also similar with the average ($\pm 1\sigma$) concentrations measured at 2.1 ± 1.3 and $1.9 \pm 1.4 \mu\text{g m}^{-3}$ at BNL and NYC, respectively. As shown in Figure 10, sulfate and LV-OOA correlated well at both locations with similar linear-regression slopes (~ 1.34 at BNL and ~ 1.47 at NYC). In addition, the polar plots of sulfate and LV-OOA at BNL demonstrate a similar pattern, showing concentration hotspots from SW (Figure 7). These results are consistent with the fact that both aerosol components are mainly formed in regional air masses.

In addition, negligible NOA was observed in oceanic air masses, consistent with our hypothesis that the NOA observed in this study was mainly associated with industrial sources. The PM_{10} composition was similar among the remaining clusters that cover the NE U.S. continent, with a larger fraction of aged secondary species, indicative of a regional source for sulfate and LV-OOA.

The west (W) cluster generally had the highest PM_{10} loading ($17.9 \mu\text{g m}^{-3}$), followed by air masses from south-southwest (SSW), due to the influence of upwind emissions from dense urban cities such as NYC, Pittsburgh, Philadelphia, Baltimore, and Washington. We also observed high CO and AVOC concentrations in the W and SSW clusters (Figures 8d and 8e). These results are consistent with the spatial distribution of emission sources of air pollutants in the NE U.S. and further demonstrate that emissions from upwind urban areas exerted substantial influence on the aerosol characteristics at BNL.

To further investigate the influence of urban emissions from upwind NYC on aerosol concentration and composition at BNL, we compared key VOCs and aerosol species for the two locations. Given comparable meteorological conditions for the summer of 2009 and 2011 in NYC (Table S3), measurements made at Queens College from 15 July to 3 August 2009 were utilized to represent conditions in NYC during the study period, where VOC concentrations were obtained from 24 h integrated VOC canister collection followed by gas chromatography–mass spectrometry analysis [Lin *et al.*, 2012], while NR- PM_{10} species and OA factors were determined from measurement data acquired with an HR-AMS [Sun *et al.*, 2011].

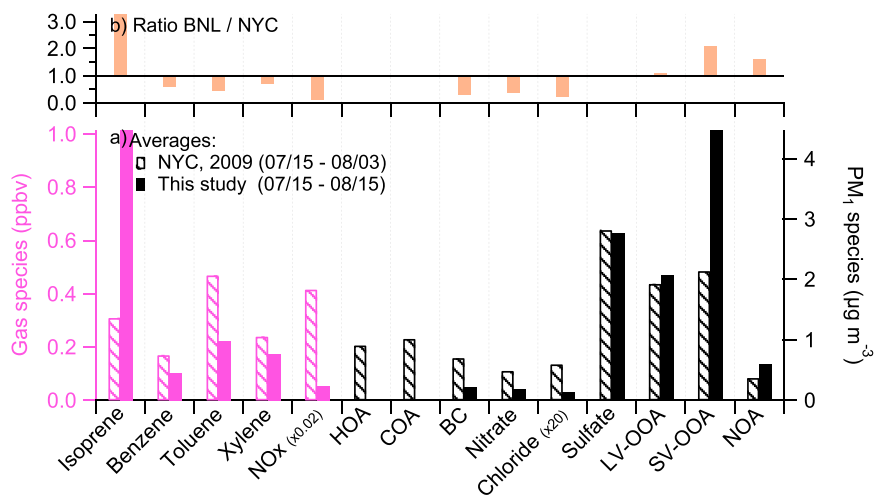


Figure 9. (a) Average concentrations of VOCs, primary particulate species, secondary particulate species, and different OA factors for NYC (striped bar) and this study (solid bar). (b) BNL/NYC ratios for each parameter.

In contrast, SV-OOA mainly represented less aged SOA observed at both BNL and NYC [Sun *et al.*, 2011]. As discussed in section 3.2.1, the SV-OOA at BNL was strongly influenced by transported urban air pollution from the W and SW directions, and its formation likely occurred both within urban plumes during transport and locally at Long Island. In addition, the mass spectra of the SV-OOA from both locations were highly similar, suggesting their chemical similarity. These findings, combined with the fact that the average SV-OOA concentration at BNL was twice that in NYC ($4.5 \mu\text{g m}^{-3}$ versus $2.14 \mu\text{g m}^{-3}$; Figure 9), suggest that the interplay between transported upwind anthropogenic emissions and local biogenic emissions contributed to the elevated SOA concentration observed at BNL. Enhancement of SOA formation in mixed anthropogenic and biogenic emissions has been found as an important aerosol process at various locations [de Gouw *et al.*, 2005; DeCarlo *et al.*, 2010; Freney *et al.*, 2014; Goldstein *et al.*, 2009; Kleinman *et al.*, 2008; Liggio *et al.*, 2010; Setyan

et al., 2012, 2014; Shilling *et al.*, 2013]. The observations from this study further indicate the importance of understanding the interactions between biogenic and anthropogenic emissions in SOA formation in the eastern U.S. in order to better understand the characteristics of aerosol particles and their effects on climate, human health, and air quality in this region.

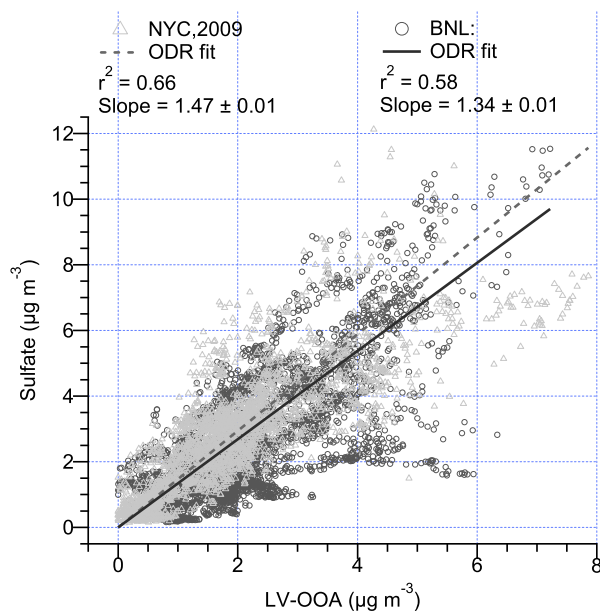


Figure 10. Scatterplot of sulfate versus LV-OOA for NYC (diamond) and this study (open circle) with ODR fitting parameters. Note that the high loading event impacted by NYC UHI was excluded for BNL data during which LV-OOA and sulfate showed a poor correlation.

4. Conclusions

The DOE sponsored ALC-IOP field campaign took place at BNL (40.871°N, 72.89°W) from 15 July to 15 August 2011. BNL is located ~80 km east of New York City, in a forest region on Long Island where aerosol chemistry is influenced by a confluence of anthropogenic, biogenic, and marine emissions with the extent of atmospheric processing depending on air mass trajectories and atmospheric transport time. During this study, a suite of real-time instruments was deployed to measure aerosols and their precursors, including an Aerodyne HR-AMS that

was operated downstream of a thermodenuder to acquire highly time-resolved data on the size-resolved composition and volatility profiles of the nonrefractory species in submicron particles (PM₁). The average ($\pm 1\sigma$) mass concentration of PM₁ was 12.6 (± 7.7) $\mu\text{g m}^{-3}$, containing 64.0% organics, 24.2% sulfate, 8.1% ammonium, 1.6% nitrate, 0.1% chloride, and 1.9% black carbon (BC). PMF analysis of the high-resolution mass spectra indicated that organic aerosol at BNL was overwhelmingly secondary, consisting of (1) a semivolatile SV-OOA (O/C = 0.54; 63% of OA mass) representative of fresher SOA mainly in association with plumes transported from the urban areas W-SW of BNL; (2) a low-volatility LV-OOA (O/C = 0.97; 29% of OA), which correlated well with sulfate and organic acids, thus likely represented more aged, regional SOA subjected to aqueous processing; and (3) a nitrogen-enriched NOA (O/C = 0.19; N/C = 0.185; 8% of OA), which was mainly composed of secondary amino compounds likely formed from industrial emissions.

The influence of anthropogenic emissions on aerosol characteristics at BNL was investigated by comparing the results of this study to an earlier field campaign conducted in NYC in July 2009. The concentrations of LV-OOA and sulfate were similar at both sites, consistent with the fact that both species were mainly formed in regional air masses. SV-OOA, however, was found to be twice higher at BNL than in NYC despite that it was clearly associated with urban emissions and showed good correlations with anthropogenic tracers such as CO, BC, NO_x, and aromatic hydrocarbons at BNL. In addition, anthropogenic tracers were all substantially lower at BNL than in NYC, while isoprene was 3 times higher. These findings, combined with back trajectory analysis of air mass origins, indicate that transported emissions from the New York metropolitan area strongly influence aerosol concentration and composition at downwind locations and that the interactions between anthropogenic and biogenic emissions may have substantially enhanced SOA formation in the eastern U.S.

Acknowledgments

This study was funded by the U.S. DOE the Atmospheric Radiation Measurement (ARM) and the Atmospheric System Research Program, Grants DE-FG02-11ER65293 and DE-SC0007178. Shan Zhou was partially funded by a PhD grant from the Chinese Scholarship Council and the Donald G. Crosby Fellowship at UC Davis. Data presented in this manuscript are available for download at the ARM data archive (<http://www.arm.gov/campaigns/osc2011aerosolife>) and at Aerosol Mass Spectrometry (AMS) Global Database (<https://sites.google.com/site/amsglobaldatabase/urban-down-wind/upton-ny-us>). Information on data analysis codes is provided in section 2.

References

- Aiken, A. C., et al. (2008), O/C and OM/OC ratios of primary, secondary, and ambient organic aerosols with high-resolution time-of-flight aerosol mass spectrometry, *Environ. Sci. Technol.*, *42*(12), 4478–4485, doi:10.1021/es703009q.
- Alfarra, M. R., D. Paulsen, M. Gysel, A. A. Garforth, J. Dommen, A. S. H. Prévôt, D. R. Worsnop, U. Baltensperger, and H. Coe (2006), A mass spectrometric study of secondary organic aerosols formed from the photooxidation of anthropogenic and biogenic precursors in a reaction chamber, *Atmos. Chem. Phys.*, *6*, 5279–5293.
- Bates, T. S., P. K. Quinn, D. J. Coffman, J. E. Johnson, and A. M. Middlebrook (2005), Dominance of organic aerosols in the marine boundary layer over the Gulf of Maine during NEAQS 2002 and their role in aerosol light scattering, *J. Geophys. Res.*, *110*, D18202, doi:10.1029/2005JD005797.
- Canagaratna, M. R., et al. (2015), Elemental ratio measurements of organic compounds using aerosol mass spectrometry: Characterization, improved calibration, and implications, *Atmos. Chem. Phys.*, *15*(1), 253–272, doi:10.5194/acp-15-253-2015.
- Carslaw, D. C. (2015), *The Openair Manual—Open-Source Tools for Analysing Air Pollution Data. Manual for Version 1.1-4*, King's College, London.
- Carslaw, D. C., and K. Ropkins (2012), Openair - an R package for air quality data analysis, *Environ. Modell. Software*, *27–28*, 52–61, doi:10.1016/j.envsoft.2011.09.008.
- Collier, S., S. Zhou, T. Kuwayama, S. Forestieri, J. Brady, M. Zhang, M. Kleeman, C. Cappa, T. Bertram, and Q. Zhang (2015), Organic PM emissions from vehicles: Composition, O/C ratio, and dependence on PM concentration, *Aerosol Sci. Technol.*, *49*(2), 86–97, doi:10.1080/02786826.2014.1003364.
- Cottrell, L. D., R. J. Griffin, J. L. Jimenez, Q. Zhang, I. Ulbrich, L. D. Ziemba, P. J. Beckman, B. C. Sive, and R. W. Talbot (2008), Submicron particles at Thompson Farm during ICARTT measured using aerosol mass spectrometry, *J. Geophys. Res.*, *113*, D08212, doi:10.1029/2007JD009192.
- Crippa, M., et al. (2013), Wintertime aerosol chemical composition and source apportionment of the organic fraction in the metropolitan area of Paris, *Atmos. Chem. Phys.*, *13*(2), 961–981, doi:10.5194/acp-13-961-2013.
- DeCarlo, P. F., et al. (2006), Field-deployable, high-resolution, time-of-flight aerosol mass spectrometer, *Anal. Chem.*, *78*(24), 8281–8289, doi:10.1021/ac061249n.
- DeCarlo, P. F., et al. (2010), Investigation of the sources and processing of organic aerosol over the Central Mexican Plateau from aircraft measurements during MILAGRO, *Atmos. Chem. Phys.*, *10*(12), 5257–5280, doi:10.5194/acp-10-5257-2010.
- de Gouw, J. A., et al. (2005), Budget of organic carbon in a polluted atmosphere: Results from the New England Air Quality Study in 2002, *J. Geophys. Res.*, *110*, D16305, doi:10.1029/2004JD005623.
- Draxler, R. R., and G. D. Hess (1998), An overview of the HYSPLIT-4 modeling system for trajectories, dispersion, and deposition, *Aust. Meteorol. Mag.*, *47*, 295–308.
- Drewnick, F., J. T. Jayne, M. Canagaratna, D. R. Worsnop, and K. L. Demerjian (2004a), Measurement of ambient aerosol composition during the PMTACS-NY 2001 using an aerosol mass spectrometer. Part II: Chemically speciated mass distributions, *Aerosol Sci. Technol.*, *38*, 104–117, doi:10.1080/02786820390229534.
- Drewnick, F., J. J. Schwab, J. T. Jayne, M. Canagaratna, D. R. Worsnop, and K. L. Demerjian (2004b), Measurement of ambient aerosol composition during the PMTACS-NY 2001 using an aerosol mass spectrometer. Part I: Mass concentrations, *Aerosol Sci. Technol.*, *38*, 92–103, doi:10.1080/02786820390229507.
- Ehn, M., et al. (2014), A large source of low-volatility secondary organic aerosol, *Nature*, *506*(7489), 476–479, doi:10.1038/nature13032.
- Ervens, B., B. J. Turpin, and R. J. Weber (2011), Secondary organic aerosol formation in cloud droplets and aqueous particles (aqSOA): A review of laboratory, field and model studies, *Atmos. Chem. Phys.*, *11*(21), 11,069–11,102, doi:10.5194/acp-11-11069-2011.
- Farmer, D. K., A. Matsunaga, K. S. Docherty, J. D. Surratt, J. H. Seinfeld, P. J. Ziemann, and J. L. Jimenez (2010), Response of an aerosol mass spectrometer to organonitrates and organosulfates and implications for atmospheric chemistry, *Proc. Natl. Acad. Sci. U.S.A.*, *107*(15), 6670–6675, doi:10.1073/pnas.0912340107.

- Fierz, M., M. G. C. Vernooij, and H. Burtscher (2007), An improved low-flow thermodenuder, *J. Aerosol Sci.*, *38*(11), 1163–1168, doi:10.1016/j.jaerosci.2007.08.006.
- Frey, E. J., et al. (2014), Characterizing the impact of urban emissions on regional aerosol particles: Airborne measurements during the MEGAPOLI experiment, *Atmos. Chem. Phys.*, *14*(3), 1397–1412, doi:10.5194/acp-14-1397-2014.
- Freutel, F., et al. (2013), Aerosol particle measurements at three stationary sites in the megacity of Paris during summer 2009: Meteorology and air mass origin dominate aerosol particle composition and size distribution, *Atmos. Chem. Phys.*, *13*(2), 933–959, doi:10.5194/acp-13-933-2013.
- Fry, J. L., et al. (2009), Organic nitrate and secondary organic aerosol yield from NO₃ oxidation of beta-pinene evaluated using a gas-phase kinetics/aerosol partitioning model, *Atmos. Chem. Phys.*, *9*(4), 1431–1449.
- Fry, J. L., et al. (2013), Observations of gas- and aerosol-phase organic nitrates at BEACHON-RoMBAS 2011, *Atmos. Chem. Phys.*, *13*(17), 8585–8605, doi:10.5194/acp-13-8585-2013.
- Ge, X. L., A. S. Wexler, and S. L. Clegg (2011), Atmospheric amines - Part I. A review, *Atmos. Environ.*, *45*(3), 524–546, doi:10.1016/j.atmosenv.2010.10.012.
- Ge, X. L., A. Setyan, Y. L. Sun, and Q. Zhang (2012a), Primary and secondary organic aerosols in Fresno, California during wintertime: Results from high resolution aerosol mass spectrometry, *J. Geophys. Res.*, *117*, D19301, doi:10.1029/2012JD018026.
- Ge, X. L., Q. Zhang, Y. L. Sun, C. R. Ruehl, and A. Setyan (2012b), Effect of aqueous-phase processing on aerosol chemistry and size distributions in Fresno, California, during wintertime, *Environ. Chem.*, *9*(3), 221–235, doi:10.1071/en11168.
- Gentner, D. R., R. A. Harley, A. M. Miller, and A. H. Goldstein (2009), Diurnal and seasonal variability of gasoline-related volatile organic compound emissions in Riverside, California, *Environ. Sci. Technol.*, *43*(12), 4247–4252, doi:10.1021/es9006228.
- Ghan, S., and S. E. Schwartz (2007), Aerosol properties and processes: A path from field and laboratory measurements to global climate models, *Bull. Am. Meteorol. Soc.*, *88*(7), 1059–1083, doi:10.1175/BAMS-88-7-1059.
- Goldstein, A. H., C. D. Koven, C. L. Heald, and I. Y. Fung (2009), Biogenic carbon and anthropogenic pollutants combine to form a cooling haze over the southeastern United States, *Proc. Natl. Acad. Sci. U.S.A.*, *106*(22), 8835–8840, doi:10.1073/pnas.0904128106.
- Heiden, A. C., K. Kobel, M. Komenda, R. Koppmann, M. Shao, and J. Wildt (1999), Toluene emissions from plants, *Geophys. Res. Lett.*, *26*, 1283–1286, doi:10.1029/1999GL900220.
- IPCC (2013), *Climate Change 2013: The Physical Science Basis. Contribution of Working Group I to the Fifth Assessment Report of the Intergovernmental Panel on Climate Change*, edited by T. F. Stocker et al., 1535 pp., Cambridge Univ. Press, Cambridge, U. K.
- Jimenez, J. L., et al. (2009), Evolution of organic aerosols in the atmosphere, *Science*, *326*(5959), 1525–1529, doi:10.1126/science.1180353.
- Jokinen, T., et al. (2015), Production of extremely low volatile organic compounds from biogenic emissions: Measured yields and atmospheric implications, *Proc. Natl. Acad. Sci. U.S.A.*, *112*(23), 7123–7128, doi:10.1073/pnas.1423977112.
- Kleinman, L. I., et al. (2008), The time evolution of aerosol composition over the Mexico City plateau, *Atmos. Chem. Phys.*, *8*(6), 1559–1575, doi:10.5194/acp-8-1559-2008.
- Lanz, V. A., M. R. Alfarra, U. Baltensperger, B. Buchmann, C. Hueglin, and A. S. H. Prévôt (2007), Source apportionment of submicron organic aerosols at an urban site by factor analytical modelling of aerosol mass spectra, *Atmos. Chem. Phys.*, *7*(6), 1503–1522.
- Liggio, J., et al. (2010), Primary and secondary organic aerosols in urban air masses intercepted at a rural site, *J. Geophys. Res.*, *115*, D21305, doi:10.1029/2010JD014426.
- Lin, Y. C., J. J. Schwab, K. L. Demerjian, M.-S. Bae, W.-N. Chen, Y. Sun, Q. Zhang, H.-M. Hung, and J. Perry (2012), Summertime formaldehyde observations in New York City: Ambient levels, sources and its contribution to HOx radicals, *J. Geophys. Res.*, *117*, D08305, doi:10.1029/2011JD016504.
- Lloyd, J. A., K. J. Heaton, and M. V. Johnston (2009), Reactive uptake of trimethylamine into ammonium nitrate particles, *J. Phys. Chem. A*, *113*(17), 4840–4843, doi:10.1021/jp900634d.
- Massoli, P., et al. (2012), Pollution gradients and chemical characterization of particulate matter from vehicular traffic near major roadways: Results from the 2009 Queens College air quality study in NYC, *Aerosol Sci. Technol.*, *46*(11), 1201–1218, doi:10.1080/02786826.2012.701784.
- Mather, J. H., and J. W. Voyles (2013), The Arm Climate Research Facility: A review of structure and capabilities, *Bull. Am. Meteorol. Soc.*, *94*(3), 377–392, doi:10.1175/BAMS-D-11-00218.1.
- Meir, T., P. M. Orton, J. Pullen, T. Holt, W. T. Thompson, and M. F. Arend (2013), Forecasting the New York City Urban Heat Island and sea breeze during extreme heat events, *Weather Forecast.*, *28*(6), 1460–1477, doi:10.1175/waf-d-13-00012.1.
- Middlebrook, A. M., R. Bahreini, J. L. Jimenez, and M. R. Canagaratna (2012), Evaluation of composition-dependent collection efficiencies for the aerodyne aerosol mass spectrometer using field data, *Aerosol Sci. Technol.*, *46*(3), 258–271, doi:10.1080/02786826.2011.620041.
- Murphy, S. M., A. Sorooshian, J. H. Kroll, N. L. Ng, P. Chhabra, C. Tong, J. D. Surratt, E. Knipping, R. C. Flagan, and J. H. Seinfeld (2007), Secondary aerosol formation from atmospheric reactions of aliphatic amines, *Atmos. Chem. Phys.*, *7*(9), 2313–2337, doi:10.5194/acp-7-2313-2007.
- Ng, N. L., et al. (2010), Organic aerosol components observed in Northern Hemispheric datasets from Aerosol Mass Spectrometry, *Atmos. Chem. Phys.*, *10*(10), 4625–4641, doi:10.5194/acp-10-4625-2010.
- Paatero, P., and U. Tapper (1994), Positive matrix factorization: A nonnegative factor model with optimal utilization of error-estimates of data values, *Environmetrics*, *5*(2), 111–126, doi:10.1002/env.3170050203.
- Peltier, R. E., A. P. Sullivan, R. J. Weber, C. A. Brock, A. G. Wollny, J. S. Holloway, J. A. de Gouw, and C. Warneke (2007), Fine aerosol bulk composition measured on WP-3D research aircraft in vicinity of the Northeastern United States - Results from NEAQS, *Atmos. Chem. Phys.*, *7*(12), 3231–3247.
- Pope, C. A., and D. W. Dockery (2006), Health effects of fine particulate air pollution: Lines that connect, *J. Air Waste Manage.*, *56*(6), 709–742.
- Rattigan, O. V., K. Civerolo, P. Doraiswamy, H. D. Felton, and P. K. Hopke (2013), long term black carbon measurements at two urban locations in New York, *Aerosol Air Qual. Res.*, *13*(4), 1181–1196, doi:10.4209/aaqr.2013.02.0060.
- Rollins, A. W., J. L. Fry, J. F. Hunter, J. H. Kroll, D. R. Worsnop, S. W. Singaram, and R. C. Cohen (2010), Elemental analysis of aerosol organic nitrates with electron ionization high-resolution mass spectrometry, *Atmos. Meas. Tech.*, *3*(1), 301–310, doi:10.5194/amt-3-301-2010.
- Sedlacek, A. J., E. R. Lewis, L. Kleinman, J. Z. Xu, and Q. Zhang (2012), Determination of and evidence for non-core-shell structure of particles containing black carbon using the Single-Particle Soot Photometer (SP2), *Geophys. Res. Lett.*, *39*, L06802, doi:10.1029/2012GL050905.
- Setyan, A., et al. (2012), Characterization of submicron particles influenced by mixed biogenic and anthropogenic emissions using high-resolution aerosol mass spectrometry: Results from CARES, *Atmos. Chem. Phys.*, *12*(17), 8131–8156, doi:10.5194/acp-12-8131-2012.
- Setyan, A., C. Song, M. Merkel, W. B. Knighton, T. B. Onasch, M. R. Canagaratna, D. R. Worsnop, A. Wiedensohler, J. E. Shilling, and Q. Zhang (2014), Chemistry of new particle growth in mixed urban and biogenic emissions - Insights from CARES, *Atmos. Chem. Phys.*, *14*(13), 6477–6494, doi:10.5194/acp-14-6477-2014.
- Shilling, J. E., et al. (2013), Enhanced SOA formation from mixed anthropogenic and biogenic emissions during the CARES campaign, *Atmos. Chem. Phys.*, *13*(4), 2091–2113, doi:10.5194/acp-13-2091-2013.

- Smith, J. N., K. C. Barsanti, H. R. Friedli, M. Ehn, M. Kulmala, D. R. Collins, J. H. Scheckman, B. J. Williams, and P. H. McMurry (2010), Observations of aminium salts in atmospheric nanoparticles and possible climatic implications, *Proc. Natl. Acad. Sci. U.S.A.*, *107*(15), 6634–6639, doi:10.1073/pnas.0912127107.
- Sorooshian, A., et al. (2006), Oxalic acid in clear and cloudy atmospheres: Analysis of data from International Consortium for Atmospheric Research on Transport and Transformation 2004, *J. Geophys. Res.*, *111*, D23S45, doi:10.1029/2005JD006880.
- Sun, Y. L., et al. (2011), Characterization of the sources and processes of organic and inorganic aerosols in New York city with a high-resolution time-of-flight aerosol mass spectrometer, *Atmos. Chem. Phys.*, *11*(4), 1581–1602, doi:10.5194/acp-11-1581-2011.
- Sun, Y. L., Q. Zhang, J. J. Schwab, T. Yang, N. L. Ng, and K. L. Demerjian (2012a), Factor analysis of combined organic and inorganic aerosol mass spectra from high resolution aerosol mass spectrometer measurements, *Atmos. Chem. Phys.*, *12*(18), 8537–8551, doi:10.5194/acp-12-8537-2012.
- Sun, Y. L., et al. (2012b), Characterization of near-highway submicron aerosols in New York City with a high-resolution aerosol mass spectrometer, *Atmos. Chem. Phys.*, *12*(4), 2215–2227, doi:10.5194/acp-12-2215-2012.
- Ulbrich, I. M., M. R. Canagaratna, Q. Zhang, D. R. Worsnop, and J. L. Jimenez (2009), Interpretation of organic components from Positive Matrix Factorization of aerosol mass spectrometric data, *Atmos. Chem. Phys.*, *9*(9), 2891–2918.
- Vladutescu, D. V., B. L. Madhavan, B. M. Gross, Q. Zhang, and S. Zhou (2013), Aerosol transport and source attribution using sunphotometers, models and in-situ chemical composition measurements, *IEEE Trans. Geosci. Remote Sens.*, *51*(7), 3803–3811, doi:10.1109/tgrs.2012.2227489.
- von der Weiden, S. L., F. Drewnick, and S. Borrmann (2009), Particle loss calculator – A new software tool for the assessment of the performance of aerosol inlet systems, *Atmos. Meas. Tech.*, *2*(2), 479–494, doi:10.5194/amt-2-479-2009.
- Weimer, S., F. Drewnick, O. Högrefe, J. J. Schwab, K. Rhoads, D. Orsini, M. Canagaratna, D. R. Worsnop, and K. L. Demerjian (2006), Size-selective nonrefractory ambient aerosol measurements during the Particulate Matter Technology Assessment and Characterization Study - New York 2004 Winter Intensive in New York City, *J. Geophys. Res.*, *111*, D18305, doi:10.1029/2006JD007215.
- White, M. L., et al. (2009), Are biogenic emissions a significant source of summertime atmospheric toluene in the rural Northeastern United States? *Atmos. Chem. Phys.*, *9*(1), 81–92.
- Young, D. E., H. Kim, C. Parworth, S. Zhou, X. Zhang, C. D. Cappa, R. Seco, S. Kim, and Q. Zhang (2016), Influences of emission sources and meteorology on aerosol chemistry in a polluted urban environment: results from DISCOVER-AQ California, *Atmos. Chem. Phys.*, *16*(8), 5427–5451, doi:10.5194/acp-16-5427-2016.
- Yu, J. Z., X.-F. Huang, J. Xu, and M. Hu (2005), When aerosol sulfate goes up, so does oxalate: Implication for the formation mechanisms of oxalate, *Environ. Sci. Technol.*, *39*(1), 128–133, doi:10.1021/es049559f.
- Yu, L., J. Smith, A. Laskin, K. M. George, C. Anastasio, J. Laskin, A. M. Dillner, and Q. Zhang (2016), Molecular transformations of phenolic SOA during photochemical aging in the aqueous phase: competition among oligomerization, functionalization, and fragmentation, *Atmos. Chem. Phys.*, *16*(7), 4511–4527, doi:10.5194/acp-16-4511-2016.
- Zhang, J., and S. T. Rao (1999), The role of vertical mixing in the temporal evolution of ground-level ozone concentrations, *J. Appl. Meteorol.*, *38*(12), 1674–1691, doi:10.1175/1520-0450(1999)038<1674:TROVMI>2.0.CO;2.
- Zhang, Q., D. R. Worsnop, M. R. Canagaratna, and J. L. Jimenez (2005a), Hydrocarbon-like and oxygenated organic aerosols in Pittsburgh: Insights into sources and processes of organic aerosols, *Atmos. Chem. Phys.*, *5*, 3289–3311.
- Zhang, Q., M. R. Canagaratna, J. T. Jayne, D. R. Worsnop, and J. L. Jimenez (2005b), Time- and size-resolved chemical composition of submicron particles in Pittsburgh: Implications for aerosol sources and processes, *J. Geophys. Res.*, *110*, D07S09, doi:10.1029/2004JD004649.
- Zhang, Q., J. L. Jimenez, D. R. Worsnop, and M. Canagaratna (2007), A case study of urban particle acidity and its influence on secondary organic aerosol, *Environ. Sci. Technol.*, *41*(9), 3213–3219, doi:10.1021/es061812j.
- Zhang, Q., J. L. Jimenez, M. R. Canagaratna, I. M. Ulbrich, N. L. Ng, D. R. Worsnop, and Y. Sun (2011), Understanding atmospheric organic aerosols via factor analysis of aerosol mass spectrometry: A review, *Anal. Bioanal. Chem.*, *401*(10), 3045–3067, doi:10.1007/s00216-011-5355-y.
- Zheng, J., Y. Ma, M. Chen, Q. Zhang, L. Wang, A. F. Khalizov, L. Yao, Z. Wang, X. Wang, and L. Chen (2015), Measurement of atmospheric amines and ammonia using the high resolution time-of-flight chemical ionization mass spectrometry, *Atmos. Environ.*, *102*, 249–259, doi:10.1016/j.atmosenv.2014.12.002.